Improved Catalytic Properties of Halohydrin Dehalogenase by Modification of the Halide-Binding Site

Lixia Tang,[‡] Daniel E. Torres Pazmiño,[‡] Marco W. Fraaije,[‡] René M. de Jong,[§] Bauke W. Dijkstra,[§] and Dick B. Janssen*[,‡]

Laboratories of Biochemistry and Biophysical Chemistry, Groningen Biomolecular Sciences and Biotechnology Institute, University of Groningen, Nijenborgh 4, 9747 AG, Groningen, The Netherlands

Received November 11, 2004; Revised Manuscript Received February 21, 2005

ABSTRACT: Halohydrin dehalogenase (HheC) from *Agrobacterium radiobacter* AD1 catalyzes the dehalogenation of vicinal haloalcohols by an intramolecular substitution reaction, resulting in the formation of the corresponding epoxide, a halide ion, and a proton. Halide release is rate-limiting during the catalytic cycle of the conversion of (*R*)-*p*-nitro-2-bromo-1-phenylethanol by the enzyme. The recent elucidation of the X-ray structure of HheC showed that hydrogen bonds between the OH group of Tyr187 and between the Oδ1 atom of Asn176 and Nϵ1 atom of Trp249 could play a role in stabilizing the conformation of the halide-binding site. The possibility that these hydrogen bonds are important for halide binding and release was studied using site-directed mutagenesis. Steady-state kinetic studies revealed that mutant Y187F, which has lost both hydrogen bonds, has a higher catalytic activity (k_{cat}) with two of the three tested substrates compared to the wild-type enzyme. Mutant W249F also shows an enhanced k_{cat} value with these two substrates, as well as a remarkable increase in enantiopreference for (*R*)-*p*-nitro-2-bromo-1-phenylethanol. In case of a mutation at position 176 (N176A and N176D), a 1000-fold lower catalytic efficiency (k_{cat}/K_m) was obtained, which is mainly due to an increase of the K_m value of the enzyme. Pre-steady-state kinetic studies showed that a burst of product formation precedes the steady state, indicating that halide release is still rate-limiting for mutants Y187F and W249F. Stopped-flow fluorescence experiments revealed that the rate of halide release is 5.6-fold higher for the Y187F mutant than for the wild-type enzyme and even higher for the W249F enzyme. Taken together, these results show that the disruption of two hydrogen bonds around the halide-binding site increases the rate of halide release and can enhance the overall catalytic activity of HheC.

Halohydrin dehalogenases catalyze the intramolecular nucleophilic displacement of a halogen by a vicinal hydroxyl group in haloalcohols, producing the corresponding epoxides. They also efficiently catalyze the reverse reaction with alternative nucleophiles (N_3^-, CN^-, NO_2^-, etc.) (*1*, *2*). The enzymes are involved in the bacterial degradation of several important environmental chemicals, such as 1,3-dichloro-2-propanol, epichlorohydrin, and 1,2-dibromoethane (*3*−*5*). The catalytic pathway of these compounds includes a step in which a vicinal halohydrin is converted to an epoxide. The halohydrin dehalogenase (HheC)[1] from *Agrobacterium radiobacter* AD1, which is the topic of this paper, converts 1,3-dichloro-2-propanol to epichlorohydrin. After hydrolysis to 1-chloro-2,3-propanediol by epoxide hydrolase, the dehalogenase converts the product to glycidol, which is further metabolized and serves as a growth substrate (*3*). The halohydrin dehalogenases differ from several other well-understood dehalogenases (*6*−*11*), such as haloalkane dehalogenases and halocarboxylic acid dehalogenases, since they do not use covalent catalysis. The enzymes, which show significant sequence and mechanistic similarity with the short-chain dehydrogenase/reductase (SDR) protein family, have recently received attention due to their ability to produce optically pure haloalcohols and epoxides and because of the broad range of nucleophiles that is accepted in epoxide ring-opening reactions (*1*, *2*, *12*, *13*).

Halohydrin dehalogenase (HheC) from *A. radiobacter* has been studied in detail (*1*, *13*, *14*, *17*, *18*, *21*). The enzyme is a homotetramer with 28 kDa subunits. HheC exhibits high activity toward a broad range of aliphatic and aromatic halohydrins. The X-ray structures of HheC with bromide bound, and with (*R*)-styrene oxide and chloride bound, as well as a structure containing the halohydrin substrate mimic (*R*)-1-*p*-nitrophenyl-2-azidoethanol (*p*NPAE), have recently been solved (*14*). The structures show that each subunit has a Rossmann fold that is typical for the short-chain dehydrogenase/reductase (SDR) protein family (*15*). The active site is located in a loop-surrounded cavity, in which a catalytic triad (Ser132, Tyr145, and Arg149) is positioned (Figure 1A). A reaction mechanism for HheC was proposed on the basis of structural similarity with SDR proteins, site-directed mutagenesis experiments, and X-ray crystallographic studies

* To whom correspondence should be addressed. Tel: (31) 50-3634209. Fax: (31) 50-3634165. E-mail: d.b.janssen@rug.nl.

[‡] Laboratory of Biochemistry, Groningen Biomolecular Sciences and Biotechnology Institute, University of Groningen.

[§] Laboratory of Biophysical Chemistry, Groningen Biomolecular Sciences and Biotechnology Institute, University of Groningen.

[1] Abbreviations: HheC, halohydrin dehalogenase; PNSHH, *p*-nitro-2-bromo-1-phenylethanol; SDR, short-chain dehydrogenase/reductase; PNSO, *p*-nitrostyrene oxide.

10.1021/bi047613z CCC: $30.25
Published on Web 04/08/2005

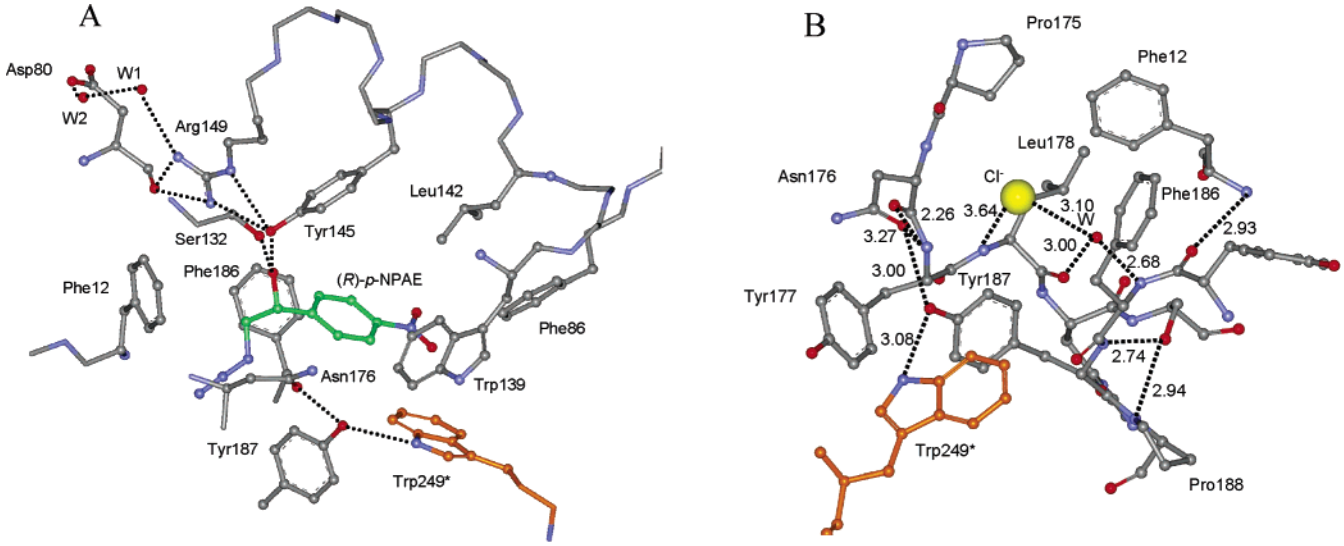

FIGURE 1: X-ray structures of the active site of halohydrin dehalogenase (HheC). (A) Structure of the active site of HheC with (*R*)-1-*p*-nitrophenyl-2-azidoethanol [(*R*)-*p*NPAE, in green] bound (PDB code 1PXO). Trp249 (in brown) is from another monomer in the tetramer. (B) Halide-binding site of HheC with a chloride ion (yellow ball) bound in the X-ray structure of the enzyme−chloride−(*R*)-styrene oxide complex (PDB code 1PWZ). Hydrogen bonds are indicated by dashed lines, and the distances are indicated by the numbers (Å).

of the enzyme cocrystallized with epoxide (*13*, *14*). The enzyme follows a general base catalysis mechanism. The conserved serine is involved in substrate binding by interacting with the hydroxyl oxygen of the substrate. The primary role of Arg149 is suggested to be lowering of the pK_a of Tyr145, which abstracts a proton from the substrate hydroxyl group to activate it for nucleophilic attack on the neighboring halogen-substituted carbon atom, resulting in release of halide and formation of an epoxide. Recently, the mechanistic role of the catalytic triad Ser114, Tyr155, and Lys159 in 3α-hydroxysteroid dehydrogenase/carbonyl reductases (3α-HSD/CR) from *Comamonas testosteroni* has been analyzed in detail (*16*). Tyr155, corresponding to Tyr145 of HheC, was proven to be an effective base in the phenolate form with an unusually low pK_a of 7.2. In HheC, Tyr145 probably also has a low pK_a as indicated by the pH dependency of the k_{cat} for 2-bromoethanol conversion (p$K_{a,app}$ = 7.3; L. Tang, unpublished data). Proton acceptance is facilitated by Lys159 in 3α-HSD/CR, which is at a position corresponding to that of Arg149 in HheC. Recently, the kinetic mechanism of HheC has been studied, using (*R*)-*p*-nitro-2-bromo-1-phenylethanol (PNSHH) as a model substrate (*17*). The conversion of (*R*)-PNSHH obeys an ordered Uni-Bi mechanism, and the inhibition pattern as well as the occurrence of burst kinetics suggested that halide is first released from the enzyme, followed by the epoxide. Moreover, substrate binding was identified as a rapid equilibrium step, and halide release appeared to be rate-limiting in the overall catalytic cycle of the forward reaction.

Crystallization of HheC with chloride ion and (*R*)-styrene oxide bound showed that the halide-binding site is mainly formed by the backbone of residues 175−178, which are in a loop region (Figure 1B). Clear interactions of the chloride ion with the enzyme can be observed (*14*). This includes contacts with the peptide nitrogen atoms of Tyr177 and Leu178 and the Cα atom of Asn176. The chloride also interacts with the side chains of Pro175, Leu178, Phe12, Phe186, and Tyr187. An interaction between the chloride ion and a water molecule that is bound at the back of the halide-binding site was also observed. The loop that forms the halide-binding site is stabilized by hydrogen bonds between Asn176 and Tyr187 and between Tyr187 and Trp249 from the other subunit. In addition, Leu178 seems to close off a possible halide exit route. Previous halide-binding studies revealed that a local conformational change occurs around the active site upon halide binding by HheC, resulting in a large increase of intrinsic protein fluorescence (*18*). The structural correlate of this fluorescence change is unknown since no structure of a ligand-free enzyme has been solved. A conformational change may also be needed for the release of halide from the active site of HheC. The deletion of the hydrogen bonds that stabilize the loop between residues 175 and 188 could possibly weaken the packing of the halide-binding site and thus facilitate the motions that are required for halide release and accelerate the catalytic cycle of the enzyme.

To test these hypotheses, site-directed mutagenesis experiments were conducted. Of the analyzed HheC mutants, variants of Leu178 did not fold correctly, whereas variants Y187F and W249F showed a higher activity toward both aliphatic and aromatic substrates and a higher rate of halide release than the wild-type enzyme. The results are in agreement with a kinetic mechanism in which halide release is rate-limiting and in which the overall catalytic rate can be enhanced by destabilizing the halide-binding loop.

MATERIALS AND METHODS

Materials. Both enantiomers of *p*-nitro-2-bromo-1-phenylethanol (PNSHH, *p*-nitrostyrene halohydrin) (99% enantiomerically pure) and *p*-nitrostyrene oxide (PNSO) (99% enantiomerically pure) were synthesized as described by Westkaemper and Hanzlik (*18*). The enantiomers of PNSHH were separated by preparative HPLC as described before (*18*). All other chemicals were of p.a. (pro analysi) quality. Oligonucleotide primers were from Sigma Genosys.

Mutagenesis. For mutagenesis the previously constructed plasmid pGEFHheC was used (*13*). It contains the *hheC* gene

(accession number AF397296) under control of the phage T7 RNA polymerase promoter. Mutant enzymes were constructed using the QuikChange site-directed mutagenesis kit of Stratagene (La Jolla, CA) with pGEFHheC as the template following the recommendations of the manufacturer. Asn176 was mutated to Ala or Asp with primers 5′-TTCGCAATAGGACCC**GCA**TATCTTCACAGTGAA or 5′-TTCGCAATAGGACCC**GAT**TATCTTCACAGTGAA. Tyr187 was changed to Phe with primer 5′-GATAGTCCCTACTTC**TTC**CCCACAGAACCGTGG. Primers 5′-GCAATAGGACCCAATTAT**GCA**CACAGTGAAGATAGTCCC and 5′-GCAATAGGACCCAATTAT**TTC**CACAGTGAAGATAGTCCC were used to obtain mutants L178A and L178F, respectively. The mutated codons are shown in bold. Mutant W249F was constructed as described before (*18*). Successful mutagenesis was confirmed by sequence analysis.

Enzyme Purification and Assay. Wild-type and mutant HheC were expressed in *Escherichia coli* BL21(DE3) and purified using Q-Sepharose (50 mL; Pharmacia Biotech) as described before (*20*). All buffers contained 10% glycerol and 1 mM β-mercaptoethanol to improve the stability of the enzyme (*21*). During purification the halohydrin dehalogenase activity was determined using the chromogenic substrate *rac-p*-nitro-2-bromophenylethanol by monitoring the absorbance change at 310 nm ($\epsilon_{PNSHH} = 3100$ cm^{-1}·M^{-1}; $\epsilon_{PNSO} = 4289$ cm^{-1}·M^{-1}) in 50 mM Tris−sulfate buffer (pH 7.5) at 30 °C on a Perkin-Elmer Lambda Bio 10 UV/vis spectrophotometer (*2*). The concentration of protein was determined by measuring the absorbance at 280 nm using an extinction coefficient of 35920 cm^{-1}·M^{-1}.

Determination of Ligand Binding by Fluorescence Titration. Fluorescence titrations were performed on a Fluorolog-3 spectrofluorometer at 30 °C with an excitation wavelength of 290 nm, and emission spectra were recorded in the range of 300−450 nm. Immediately prior to the experiment, the enzyme was diluted to a desired concentration. Halide and other nucleophiles were added from freshly prepared stock solutions in 50 mM Tris−sulfate buffer (pH 8.0) containing 1 mM β-mercaptoethanol to protein solutions (0.03 mg/mL). Apparent dissociation constants were obtained by nonlinear regression fitting of eq 1 using SigmaPlot 2000 as described

$$\Delta F = f_a[S]/([S] + K_d) \quad (1)$$

before (*18*). In this equation, ΔF is the relative change of the fluorescence intensity at λ_{Emax}, [S] is the concentration of halide, epichlorohydrin, or another ligand, K_d is the apparent dissociation constant, and f_a is the relative change of the fluorescence intensity at [S] $\gg K_d$.

Steady-State Kinetics. The steady-state kinetic parameters with 1,3-dichloro-2-propanol were determined in 50 mM Tris−sulfate buffer (pH = 8.0) at 30 °C by either monitoring halide liberation (*22*) or gas chromatography (*12*). Halohydrins and epoxides were analyzed by gas chromatography. Samples (1.5 mL) were extracted with 1.5 mL of diethyl ether containing 0.05 mM mesitylene as an internal standard. Extracts were analyzed by split injection of 2 μL on a HP5 column (model HP 19091J-413; Hewlett-Packard) with helium as a carrier gas. For the chromogenic substrate *p*-nitro-2-bromophenylethanol, the initial velocities were measured as described before (*18*). Data were fitted to the Michaelis−Menten equation using nonlinear regression.

Scheme 1

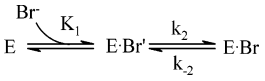

Circular Dichroism Spectroscopy. Far-UV CD spectra were recorded from 190 to 250 nm at 25 °C on an AVIV model 62A DS circular dichroism spectrometer using a 0.1 cm cuvette containing 0.1 mg/mL halohydrin dehalogenase in 5 mM potassium phosphate, pH 7.5. Each spectrum shown represents the average of five scans and was corrected for the absorbance caused by the buffer.

Stopped-Flow Experiments. Stopped-flow fluorescence experiments were used to study the kinetics of bromide binding and dissociation. The experiments were done at 30 °C on an Applied Photophysics model SX17MV stopped-flow apparatus as described previously (*17*). The concentrations mentioned in the text are the concentrations after mixing. Each trace shown is the average of four to six repeated experiments. Immediately prior to the experiment, the enzyme was diluted to the required concentration with 50 mM Tris−sulfate buffer (pH 7.5) containing 1 mM β-mercaptoethanol to protect the enzyme against inactivation.

Rapid-Quench Experiments. Pre-steady-state burst formation of (*R*)-PNSO from PNSHH was measured on a Kintek RQF-63 rapid-quench apparatus at 30 °C in 50 mM Tris−sulfate buffer (pH 7.5) containing 1 mM β-mercaptoethanol. The reactions were initiated by rapidly mixing equal volumes (50 μL) of a solution of (*R*)-PNSHH (1.5 mM, final concentration) and an enzyme solution (0.12 mM Y187F or 0.087 mM W249F). The reaction mixtures were then quenched with 0.4 M H_2SO_4 (final concentration). To prevent chemical conversion of PNSO under these acidic conditions, the quenched reaction mixtures were directly injected into a tube containing 0.7 mL of 1 M phosphate buffer (pH 7.6) and 1.5 mL of diethyl ether with mesitylene as an internal standard. Quantitative analysis of PNSO in the ether phase was performed by HPLC using an analytical Chiralcel OD column with heptane/2-propanol (92:8) as eluent (1.3 mL/min). The retention times of (*R*)-PNSO and (*R*)-PNSHH were 8.3 and 16.8 min, respectively.

Data Analysis. Stopped-flow traces of bromide-binding experiments were fitted using nonlinear regression analysis (SigmaPlot version 8.0 for Windows) to a single exponential equation, resulting in k_{obs} values for different bromide concentrations.

$$F = A(1 - e^{k_{obs}t}) \quad (2)$$

The individual rate constants in Scheme 1 were obtained by fitting eq 3 to the experimental k_{obs} values using the program Scientist (MicroMath). This led to a unique set of solutions for the rate and equilibrium constants that could describe the fluorescence traces over the whole concentration range.

$$k_{obs} = k_{-2} + \frac{k_2[Br]}{[Br] + K_1} \quad (3)$$

Assuming that the bromide-bound enzyme E·Br in Scheme 1 is responsible for the elevated fluorescence intensity, the steady-state fluorescence can be expressed as a function of the constants in Scheme 1:

$$F = F_0 + f_a F_0 \frac{k_2[\mathrm{Br}]}{K_1 k_{-2} + [\mathrm{Br}](k_2 + k_{-2})} \quad (4)$$

where F_0 is the fluorescence intensity of the ligand-free enzyme and f_a is the relative change of the fluorescence intensity at $[Br^-] \gg K_d$.

The apparent dissociated constant is then given by the equation:

$$K_d = \frac{K_1 k_{-2}}{k_2 + k_{-2}} \quad (5)$$

For the analysis of burst kinetics of the conversion of (*R*)-PNSHH by HheC (Scheme 2), which was measured at $[S] \gg K_{mPNSHH}$, the rapid-quench data were fitted with eq 6, using the program Scientist (*23*).

$$([E{\cdot}Br{\cdot}PNSO] + [PNSO])/E_{tot} = A_0(1 - e^{-\lambda t}) + k_{cat}t \quad (6)$$

$$A_0 = \frac{k_{2c}(k_{2c} + k_{-2c})}{(k_{2c} + k_{-2c} + k_{3c})(k_{2c} + k_{-2c} + k_{3c})} \quad (7)$$

$$\lambda = k_{2c} + k_{-2c} + k_{3c} \quad (8)$$

In this equation λ is the observed burst rate constant, A_0 is the amplitude, and k_{cat} is the steady-state turnover number. Equations 7 and 8, which give the amplitude and apparent rate constant of the burst as a function of the rate constants in Scheme 2, were used to replace λ and A_0 in eq 6 for the fitting process. A unique solution of the rate constant k_{3c} was obtained for mutants Y187F and W249F, while it was difficult to obtain a precise value for k_{2c} due to a very fast ring closure of (*R*)-PNSHH by the two mutants.

Equation 9 was derived as described before (*24*). It defines the K_m value as a function of the rate constants in Scheme 2, and it was used to calculate the K_s for the binding of (*R*)-PNSHH by the mutant enzymes.

$$K_{mPNSHH} = \frac{K_s(k_{-2c} + k_{3c})}{k_{2c} + k_{-2c} + k_{3c}} \quad (9)$$

RESULTS

Mutants with a Modified Halide-Binding Site. We constructed mutants in which the hydrogen bonds that were hypothesized to influence the stability of the halide-binding site loop were disrupted. Asn176, which has a hydrogen bond with Tyr187 (Figure 1B), was replaced by an alanine or an aspartate (N176A and N176D), and Tyr187, which is hydrogen bonded to Asn176 and Trp249, was replaced by a phenylalanine (Y187F). Leu178, which was proposed to be involved in the halide release pathway in HheC, was mutated to Ala and Phe. The mutants, including the previously constructed mutant W249F (*18*), were expressed in *E. coli* BL21(DE3), and all showed similar expression levels as the wild-type enzyme. The mutant proteins could be purified via one-step purification, resulting in pure proteins (>90%) as judged by SDS−PAGE (*20*). Far-UV CD spectra of the mutant proteins were similar to that of the wild-type enzyme, showing that the mutations had no significant influence on the secondary structure of the protein. All mutants were catalytically active, with the exception of the L178A and L178F mutant proteins, which mainly were present as dimers and not studied further. The active mutants were subjected to kinetic analysis.

Scheme 2

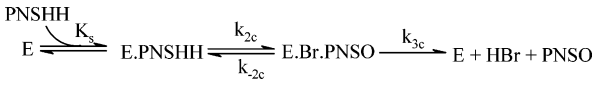

Table 1: Apparent Dissociation Constants (K_d) of HheC and Its Mutants for Anions at pH 7.5

	K_d (mM)			
enzyme	Cl^-	Br^-	CN^-	N_3^-
WT	3.1 ± 0.8	0.5 ± 0.1	1.2 ± 0.3	1.3 ± 0.2
Y187F	1.3 ± 0.6	0.3 ± 0.1	−[a]	1.9 ± 0.6
W249F	3.9 ± 1.2	0.7 ± 0.2	10.4 ± 3.4	1.2 ± 0.4

[a] No fluorescence change upon ligand addition.

Steady-State Ligand Binding. The effect of the mutations on ligand binding was measured using fluorometric titration (Table 1). Mutants Y187F and W249F showed a clear fluorescence enhancement when halide was added, similar to what is observed with the wild-type enzyme. Only a very small fluorescence increase was observed for the asparagine mutants (N176A and N176D). Thus, ligand binding could only be studied with wild-type HheC and mutants Y187F and W249F. For these proteins, the effect of halide ions (Br^- and Cl^-) and two alternative nucleophiles accepted by the enzyme (N_3^- and CN^-) on the intrinsic protein fluorescence was measured at different concentrations. The wild-type HheC showed the lowest K_d value for bromide (0.5 mM). The K_d values for N_3^- and CN^- were 2-fold higher, whereas the K_d value for chloride was about 6-fold higher than that for bromide. The mutants Y187F and W249F displayed similar dissociation constants with halides (Cl^- and Br^-) and N_3^- as the wild-type enzyme. The exception is CN^-, for which a 9-fold higher K_d value was obtained with mutant W249F than with the wild-type enzyme. No significant fluorescence change was observed when CN^- was mixed with mutant Y187F. Moreover, the wild-type enzyme displayed a similar K_d value for bromide in the absence and presence of 10 mM CN^-. The results indicate that mutating Y187F or W249F has little effect on the affinity of the ligand-binding site of HheC and that CN^- might bind to the active site in a different way than the other anions. The latter observation is in agreement with the finding that halide ions and N_3^- are inhibitors of the conversion of (*R*)-PNSHH, while CN^- (10 mM) does not inhibit the reaction (*2*).

Steady-State Kinetics. The steady-state kinetic parameters of the mutants were determined using an aliphatic and an aromatic halohydrin as the substrate (Table 2). Mutants N176A and N176D showed a more than 100-fold decrease of catalytic efficiency (k_{cat}/K_m) with the tested halohydrin substrates, but most of the k_{cat} values were reduced less, indicating that the mutations on position 176 mainly affect substrate capture by HheC.

Mutant Y187F displayed a remarkable increase of the k_{cat} value with two substrates as compared to the wild-type enzyme. With 1,3-dichloro-2-propanol, a 2-fold higher k_{cat} and a similar K_m value were obtained as with wild-type HheC, resulting in an improvement of the catalytic efficiency.

Table 2: Steady-State Kinetic Parameters of Active HheC Variants[a]

	1,3-dichloro-2-propanol			(*R*)-PNSHH			(*S*)-PNSHH			
enzyme	k_{cat} (s^{-1})	K_m (mM)	k_{cat}/K_m (M^{-1} s^{-1})	k_{cat} (s^{-1})	K_m (mM)	k_{cat}/K_m (M^{-1} s^{-1})	k_{cat} (s^{-1})	K_m (mM)	k_{cat}/K_m (M^{-1} s^{-1})	*E*
WT	9.3 ± 0.9	0.010 ± 0.002	9.3×10^5	22 ± 1	0.009 ± 0.003	2.4×10^6	7 ± 1	0.43 ± 0.05	1.6×10^4	150
N176A	>3.3	>3.2[b]	1.0×10^3	>0.76	>1.4[b]	4.6×10^2	$>7.2 \times 10^{-3}$	>0.89[a]	8.3	60
N176D	>0.97	>4.4[b]	2.3×10	>6.3	>1.5[b]	4.7×10^3	>0.2	>1.26[a]	1.7×10^2	30
Y187F	18.7 ± 1.1	0.012 ± 0.005	1.6×10^6	89 ± 3	0.17 ± 0.02	5.2×10^5	9.1 ± 0.5	0.65 ± 0.01	1.4×10^4	40
W249F	16.0 ± 0.9	0.024 ± 0.007	6.7×10^5	170 ± 13	0.05 ± 0.01	3.3×10^6	2.3 ± 0.2	0.61 ± 0.08	3.8×10^3	900

[a] The enantioselectivity toward PNSHH is expressed as the *E* value $[(k_{cat}/K_m)_R/(k_{cat}/K_m)_S]$. [b] The values are the highest substrate concentrations that were used.

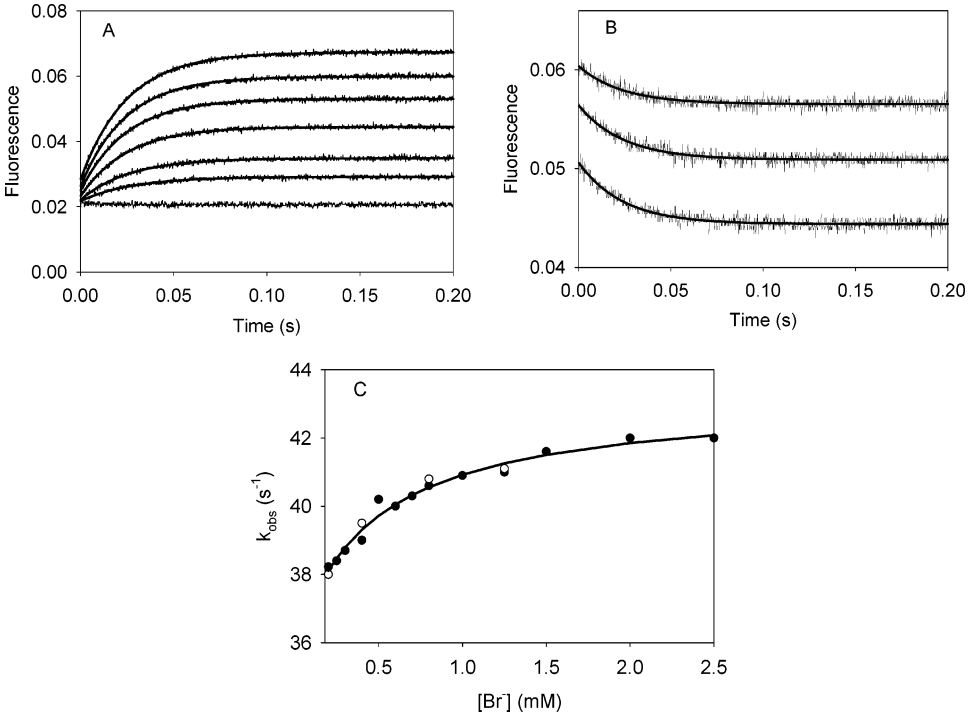

FIGURE 2: Kinetics of bromide binding and release with wild-type HheC. (A) Fluorescence traces obtained upon binding of bromide to the wild-type enzyme with a final concentration of 2.5 μM. The final concentrations of bromide are 0, 0.1, 0.2, 0.5, 1, 2, and 7 mM, respectively (from bottom to top). The solid lines represent the best fit with a single exponential function. (B) Fluorescence traces of the release of bromide from wild-type HheC. HheC (5 μM) was premixed with bromide and diluted 1 to 1 with 50 mM Tris−sulfate buffer (pH 7.5) containing 1 mM β-mercaptoethanol. The final concentration of bromide is 0.2, 0.4, and 0.8 mM (from bottom to top). The solid lines are the best fit to a single exponential function. (C) Concentration dependence of the k_{obs} for bromide binding (●) and bromide release (○). The solid line is the best fit to Scheme 1 using the data in Table 3.

For (*R*)-PNSHH, a 4-fold increase of the k_{cat} value was observed, although the catalytic efficiency was lower than with the wild-type enzyme due to a higher K_m value. The mutation on position 187 affected the steady-state kinetics toward the (*S*)-enantiomer of PNSHH in a different manner as with the (*R*)-enantiomer, since with (*S*)-PNSHH the k_{cat} and the K_m value were only slightly influenced.

Enhanced k_{cat} values for 1,3-dichloro-2-propanol and (*R*)-PNSHH, but not for (*S*)-PNSHH, were also observed for mutant W249F (Table 2). Compared to the wild-type enzyme, mutant W249F exhibited a 1.4-fold increase in catalytic efficiency (k_{cat}/K_m) for (*R*)-PNSHH, while the k_{cat}/K_m value with 1,3-dichloro-2-propanol was slightly decreased due to a 2.4-fold higher K_m value. Moreover, mutant W249F showed a remarkable 6-fold improvement of the enantioselectivity with PNSHH due to a decreased catalytic efficiency with the (*S*)-enantiomer.

Taken together, these results indicate that the catalytic rate of HheC was indeed improved by removing a hydrogen bond between Asn176 and Tyr187 or between Tyr187 and Trp249.

Pre-Steady-State Bromide Binding and Dissociation. Previous studies showed that the halide release step is rate-limiting in the catalytic cycle of the conversion of the (*R*)-PNSHH by wild-type HheC (*17*). To investigate whether the elevated k_{cat} values of mutants Y187F and W249F were caused by faster halide release, the pre-steady-state bromide binding and dissociation kinetics with these two mutants and wild-type HheC were studied by stopped-flow methods, monitoring the intrinsic protein fluorescence.

(A) Wild-Type HheC. Fluorescence traces were measured after rapid mixing of the enzyme with various concentrations of bromide (Figure 2A). It was found that the fluorescence intensity increased to a steady-state level within the first 70 ms after mixing. The traces could be fitted with a single exponential equation, yielding an observed rate constant (k_{obs}) and an amplitude. The k_{obs} values increased with increasing bromide concentrations, which can be explained by Scheme

Table 3: Kinetic Parameters of Wild-Type HheC and Mutants W187F and W249F at pH 7.5[a]

	Scheme 1					Scheme 2				
enzyme	K_d (mM)	K_{dcalc}[b] (mM)	K_1 (mM)	k_2 (s^{-1})	k_{-2} (s^{-1})	k_{cat} (s^{-1})	K_s[d] (mM)	k_{2c} (s^{-1})	k_{-2c} (s^{-1})	k_{3c} (s^{-1})
WT	0.5 ± 0.1	0.38	0.45 ± 0.1	7 ± 1	36 ± 1	22 ± 1	0.1	380	<5	21 ± 1
Y187F	0.3 ± 0.1	0.37	0.47 ± 0.1	55 ± 1	201 ± 2	89 ± 3	2.9−4.8	1500−2500	<20	92 ± 1
W249F	0.7 ± 0.2	—[c]	—[c]	—[c]	—[c]	170 ± 13	>1.2	>4000	<10	180 ± 5

[a] See Schemes 1 and 2 for definition of constants. [b] K_d values were calculated by using eq 5 and the rate constants from Table 3. [c] Not detectable due to very fast halide binding. [d] K_s values of the mutant enzymes were calculated by using eq 9.

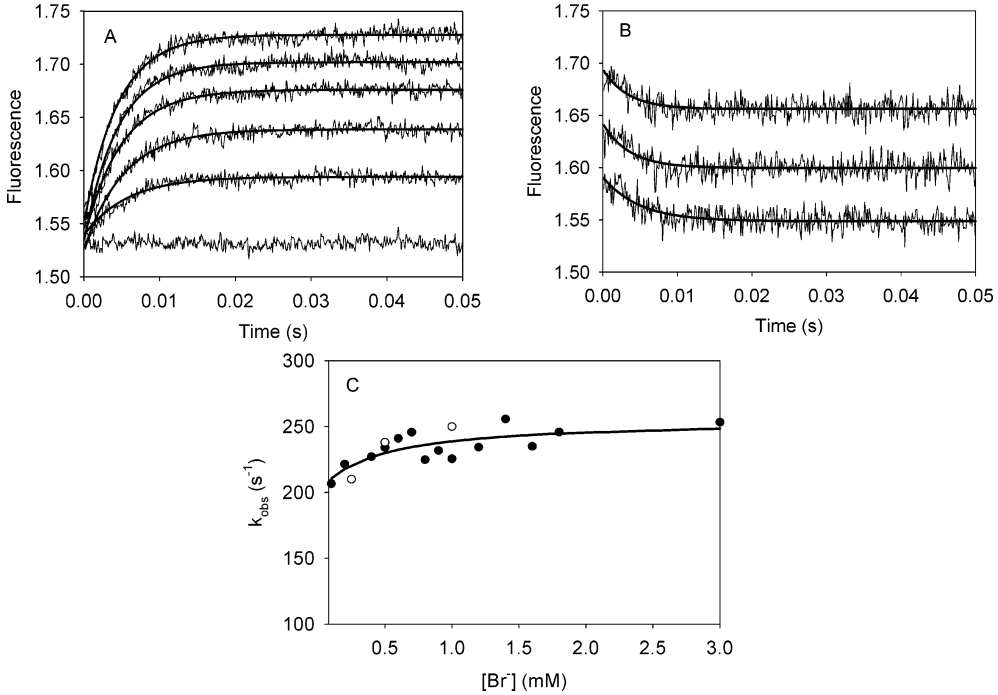

FIGURE 3: Kinetics of bromide binding and release with mutant Y187F. (A) Fluorescence traces that were obtained upon binding of bromide to mutant Y187F (5 μM). The final concentrations of bromide are 0, 0.2, 0.6, 1, 2, and 5 mM, respectively (from bottom to top). The solid lines show the fit with a single exponential function. (B) Fluorescence traces of the release of bromide from mutant Y187F. Enzyme (10 μM) was premixed with bromide and diluted 1 to 1 with 50 mM Tris−sulfate buffer (pH 7.5) containing 1 mM β-mercaptoethanol to final bromide concentrations of 0.25, 0.5, and 1 mM (from bottom to top). The solid lines are the best fit to a single exponential function. (C) Concentration dependence of the k_{obs} for bromide binding (●) and bromide release (○). The solid line is the best fit to Scheme 1 using the data in Table 3.

1, involving a rapid bimolecular binding step followed by a slow unimolecular isomerization (*23*, *25*). For bromide dissociation, all fluorescence traces could also be fitted to a single exponential equation. When the enzyme was premixed with bromide, no clear burst in fluorescence intensity was observed upon dilution with buffer, which indicates that release of bromide follows Scheme 1 as well (Figure 2B). In the case of bromide binding, the maximum value of k_{obs} that can be reached is $k_2 + k_{-2}$ (Figure 2C).

The k_{obs} values were fitted with eq 3, resulting in unique solutions for the rate and equilibrium constants in Scheme 1 (Table 3). Since no burst in fluorescence was observed upon binding of bromide by HheC, the fluorescence of enzyme E·Br′ was assumed to be equal to that of E. According to Scheme 1 and the data in Table 3, the rate of binding of bromide is mainly limited by k_2, while k_{-2} determines the release of halide. The rate of halide release (k_{-2}) for the wild-type enzyme is in the same order of magnitude as the k_{cat} value (21 s^{-1}) for the conversion of (*R*)-PNSHH. The K_d value calculated from the results of pre-steady-state kinetic studies using eq 5 was in good agreement with the value obtained from steady-state measurements (Table 3). This indicates that Scheme 1 and the corresponding rate and binding constants give a good description of the kinetic mechanism for bromide binding and release by HheC.

(B) Mutant Y187F. The pre-steady-state bromide binding and release experiments were also performed with mutant Y187F. This gave similar fluorescence traces as with the wild-type enzyme (Figure 3A), which could also be fitted with a single exponential equation. Analysis of the k_{obs} values of these traces revealed a similar bromide concentration dependent pattern (Figure 3C) as for the wild-type enzyme, which indicates a similar kinetic mechanism for bromide binding for mutant Y187F and wild-type HheC (Scheme 1). However, the k_{obs} values for mutant Y187F were much higher than those for the wild-type enzyme at the same bromide concentrations. The k_{obs} increased hyperbolically from 210 to 250 s^{-1} with increasing bromide concentrations. Bromide dissociation experiments with mutant Y187F were also performed by dilution of the bromide-premixed enzyme with buffer (Figure 3B). The relatively high noise to signal ratio is due to the smaller change of the protein fluorescence intensity upon bromide binding for mutant Y187F than for the wild-type enzyme. All fluorescence traces could again be fitted to a single exponential equation, and no fluorescence jump occurred upon dilution of the premixed enzyme.

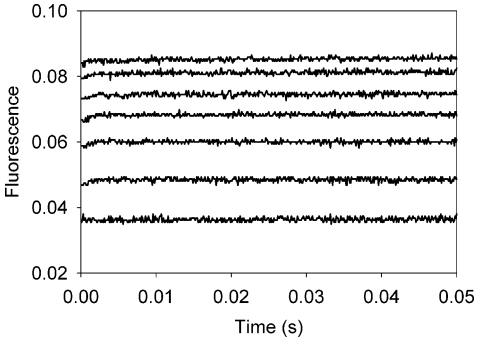

FIGURE 4: Kinetics of bromide binding with mutant W249F. Fluorescence traces obtained upon mixing bromide with mutant W249F (2 μM). The final concentrations of bromide are 0, 0.2, 0.4, 0.6, 1, 2, and 2.5 mM, respectively (from bottom to top).

The rate constants in Scheme 1 for mutant Y187F were obtained by analyzing the experimental data in the same way as for the wild-type enzyme (Table 3). For mutant Y187F, k_{-2}, which largely determines the kinetics of bromide release in the case of the wild-type enzyme, indeed is much larger than that for the wild-type enzyme. The rate of k_2 is 8-fold higher as well. The apparent halide dissociation constant (K_d) calculated by using eq 5 is similar to the one obtained from steady-state measurements.

(C) Mutant W249F. The pre-steady-state bromide-binding experiments were also performed for purified mutant W249F enzyme (Figure 4). The fluorescence intensity increased rapidly upon bromide binding, and it terminated within the dead time of stopped-flow apparatus (1.8 ms). Therefore, it is not possible to analyze the kinetics of bromide binding and dissociation for this mutant in a similar way as for the other two enzymes. However, by inspection of the fluorescence traces of wild-type HheC and the mutants, it appeared that the fluorescence intensity reached a steady-state level within 0.05 s for the wild-type enzyme, while this occurred within 0.01 and 0.002 s (dead time of the apparatus) for mutants Y187F and W249F, respectively (Figures 3A and 4). Thus, it is reasonable to conclude that mutant W249F has an even faster rate of halide binding and release than mutant Y187F.

Pre-Steady-State Burst Kinetics. To determine whether the halide release step is still rate-limiting in the catalytic cycle of conversion of (*R*)-PNSHH by mutants Y187F and W249F, pre-steady-state experiments were performed using the rapid-quench method. A pre-steady-state burst of formation of PNSO followed by a steady-state phase was obtained both with the wild-type enzyme and with the two mutants (Figure 5). This indicates that the rate-limiting step during the catalytic cycle occurs after the chemical epoxide-formation step with all of these three enzymes. Thus, product release remains the rate-limiting step in the catalytic cycle of conversion of (*R*)-PNSHH by the mutant enzymes.

The two mutants were assumed to have a similar kinetic mechanism as the wild-type enzyme, which involves three steps, with the second product being released immediately after the first one (Scheme 2) (*17*). To obtain the rate constants in Scheme 2, eq 6 was expressed as a function of rate constants by substitution of A_0 and λ with eqss 7 and 8, and then it was used to fit the rapid-quench experimental data. It was found that the value of the rate constant of k_{2c} was not well defined for the two mutants (Y187F and W249F) because of insufficient data within the first millisecond of the reaction due to the dead time of the rapid-quench apparatus. With the two mutants, the rate of the back-reaction of the chemical step (step 2 in Scheme 2) was much lower than its forward reaction, which is also the case for the wild-type enzyme. The rate of k_{3c} that determines the rate of the steady-state phase is in good agreement with the k_{cat} value obtained from steady-state measurements (Table 3).

The k_{2c} values of mutants Y187F and W249F were significantly increased compared to the wild-type enzyme, indicating that the enhanced rate of halide release for mutants Y187F and W249F is accompanied by an increased rate of dehalogenation for (*R*)-PNSHH. The values for the (*R*)-PNSHH binding constant K_s of the two mutants calculated using eq 9 with the K_m value obtained from steady-state kinetic studies and the rate constants in Table 3 (Y187F, 2.9 mM < K_s < 4.8 mM; W249F, K_s > 1.2 mM) were more than 10-fold higher than the K_s of the wild-type enzyme (0.1 mM). These results indicate that the substrate-binding step for these mutants is weaker than with the wild-type enzyme, which produces a negative effect on the catalytic efficiency of the enzyme. Thus, it is likely that the presence of the two hydrogen bonds is important for the stabilization of the structure of the Michaelis complex.

DISCUSSION

The work presented here describes a kinetic analysis of the role of residues Asn176, Tyr187, and Trp249 in halide

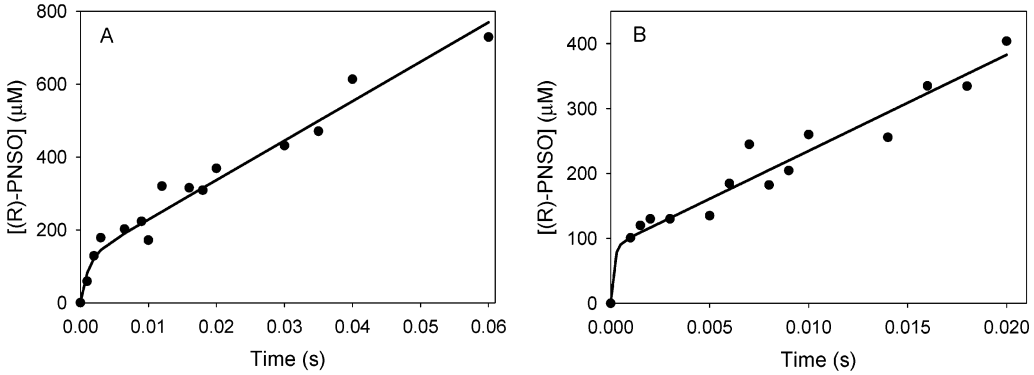

FIGURE 5: Burst kinetics of the ring-closure reaction of (*R*)-PNSHH by mutant HheC. The conversion of 1.5 mM (*R*)-PNSHH by (A) 0.12 mM Y187F and (B) 0.087 mM W249F in 50 mM Tris−sulfate buffer (pH 7.5) was followed by rapid-quench analysis after different incubation times. The solid lines are the best fit to Scheme 2 using the data in Table 3.

binding and catalytic activity of HheC. These residues are proposed to stabilize the overall conformation of the halide-binding site by forming two hydrogen bonds (Figure 1B). Steady-state kinetic studies indicated that substitution of Tyr187 or Trp249 by a phenylalanine significantly enhances the activity toward the aromatic halohydrin (*R*)-PNSHH. Moreover, pre-steady-state kinetic analysis of mutants Y187F and W249F revealed that halide release is still rate-limiting in the conversion of (*R*)-PNSHH, and therefore we assume that these two mutants follow a similar kinetic mechanism as the wild-type enzyme (Scheme 2). The results indicated that the improved catalytic activity is due to an enhanced rate of halide release for the two mutants since halide release was identified as the rate-limiting step in the conversion of (*R*)-PNSHH by the wild-type enzyme. For 1,3-dichloro-2-propanol and (*S*)-PNSHH, a less pronounced effect on the k_{cat} value was observed than with (*R*)-PNSHH, which indicates that there are differences in the kinetic mechanism for these substrates. It should also be noted that halide release in the wild-type enzyme precedes release of epoxide, which implies that the halide release step may be slower in the catalytic cycle than when it is measured in the absence of epoxide.

To prove that the release of halide is indeed enhanced for the two mutants, the pre-steady-state kinetics of halide binding was studied. The results clearly indicate that the isomerization step (k_{-2}) in the halide release pathway (Scheme 1), which determines the overall rate of halide release for both wild-type HheC and the Y187F mutant, still exists. However, its rate is much higher in the mutant. This indicates that the breakage of the two hydrogen bonds indeed enhances halide release. The observation that halide release, albeit faster, is still the slowest step in the catalytic cycle indicates that it requires more extensive structural rearrangements than just the breakage of two hydrogen bonds. Since both the bromide-free wild-type enzyme and the mutant enzymes did not crystallize, no structures are available that would help to describe the halide exit pathway further.

The involvement of a unimolecular isomerization step in the halide release pathway indicates that the halide ion produced from the hydrophobic substrate cannot be released from the occluded active site by free diffusion through the protein. Instead, the kinetic data suggest that the protein has to undergo a conformational change before halide dissociation takes place. A halide release pathway with a slow isomerization step preceding release also occurs with haloalkane dehalogenase from *Xanthobacter autotrophicus* (DhlA) (*26*). In this case, the conformational change was proposed to occur in the cap domain and to lead to solvation of the active site that facilitates halide to escape (*27*). A similar process could possibly occur in HheC, although at present there is little evidence for this. An alternative way of facilitating halide release in HheC could be an interaction with one or more positively charged residues along a halide exit channel. In the light-driven chloride pump halorhodopsin, the channel-lining arginine residue 108 was found to be essential for chloride uptake from the extracellular side and release to the interior (*28*). However, no arginine or lysine close to the halide-binding site is observed in the structure of HheC.

We further inspected the X-ray structure of wild-type HheC with bound halide and epoxide for possible routes of halide release (*14*). The halide-binding site with chloride ion bound was highlighted in Figure 1B. In the structure of the HheC·Br^-·styrene epoxide complex, stryrene epoxide closes the entrance to the halide-binding site from the solvent. It is most likely that halide is released to the solvent via a pathway lined by the water molecule in the back of halide-binding site, which is the shortest route to reach the solvent. Opening of this pathway could possibly involve a rotation around the Cα−Cβ bond of residue Leu178. Direct proof for this route is difficult to obtain as the L178A and L178F mutations not only yielded inactive enzyme but also disrupted the oligomeric state of the enzyme. A second possibility is a pathway that is close to the substrate-binding site. The two studied hydrogen bonds are located near the beginning of the substrate entrance tunnel at the protein surface. However, to allow halide release via this route with epoxide remaining bound, the tunnel needs to be enlarged by moving away several amino acids, including Tyr187 and Trp249. Thus, halide release according to this route would indeed require a conformational change that involves the amino acids targeted in this study. The release of halide via this route is in agreement with the kinetic properties of the mutant enzymes (Y187F and W249F). However, from the available X-ray structures of HheC it is difficult to envision how this conformational change precisely would happen.

The mutations at positions 187 and 249 did not cause a significant effect on the halide-binding site itself, since the K_d values of the two mutants with halide ions are similar to that of the wild-type enzyme. This is not surprising as many other interactions between the halide ion and the enzyme remain. The mutations on position 176 (N176A and N176D) caused a larger increase of the K_m value for all tested substrates than the mutations Y187F and W249F, which might be due to an effect on substrate binding. The X-ray structure revealed that the backbone and side chain atoms of Asn176 interact with the substrate mimic (*R*)-1-*p*-nitrophenyl-2-azidoethanol (*p*NPAE) via van der Waals contacts (Figure 1A), and the increase in K_m of the N176A mutant could be due to the absence of these van der Waals connections. Alternatively, there are other conformational changes in the N176A mutant that influence substrate binding. The increased K_m of the N176D mutant might be caused by the introduction of a charge in the substrate-binding pocket.

Release of halide is enhanced by the removal of the two hydrogen bonds, resulting in a large improvement of the catalytic activity of the resulting HheC mutants. Besides this, the chemical reaction step (k_{2c}), which is the actual dehalogenation reaction of (*R*)-PNSHH, also becomes much faster with mutants Y187F and W249F than with the wild-type enzyme. This observation is in contrast with the situation for haloalkane dehalogenase (DhlA). With DhlA, a higher rate of halide release is always accompanied by a lower rate of carbon−halogen cleavage in the conversion of good substrates, such as 1,2-dibromoethane and 1,2-dichloroethane (*29*), indicating that rapid carbon−halogen bond cleavage and fast halide release have opposite structural requirements and that the balance between these processes is evolutionarily optimized for 1,2-dichloroethane in DhlA. The consequence is that the halide release and the carbon−halogen cleavage steps cannot be changed independently. Apparently, carbon−halogen bond cleavage and halide release are not inversely

connected in the same way in HheC, at least for the substrates tested here, which makes it possible to obtain HheC variants with improved catalytic properties by site-directed mutagenesis.

Strikingly, the W249F mutation caused a significant improvement of the enantioselectivity with PNSHH. Most studies on increasing and changing enantioselectivity of enzymes by mutagenesis have been done with lipases and phosphotriesterase. Although several lipases with improved enantioselectivity were obtained by single point mutation, most of them possess lower catalytic activity than the corresponding wild-type enzyme (*30*). In these cases, the enhanced enantioselectivity by the mutations was due to the modifications of the substrate-binding pocket of the enzyme. In phosphotriesterase, the enantioselectivity can also be modified by site-directed mutagenesis of the residues surrounding the binding pockets for the groups bound to the chiral phosphorus atom (*31*). No such binding pockets for the substituents present on the chiral carbon atom exist in HheC, and at this moment stereoselectivity can only be interpreted in kinetic terms. In a previous paper, we demonstrated that the high enantioselectivity of wild-type HheC is mainly determined by differences in the substrate-binding step and the chemical reaction step for the two enantiomers of PNSHH (*17*). For mutant W249F, the improvement of the dehalogenation step might be one of the main causes for the enhanced enantioselectivity toward PNSHH, although the substrate-binding step is somewhat weaker than with the wild-type enzyme. Moreover, the decreased catalytic efficiency of the mutant W249F toward the (*S*)-enantiomer of PNSHH might also contribute to the improved enantioselectivity. Thus, mutant W249F represents an interesting example on the elevation of both catalytic activity and enantioselectivity by a point mutation, which is possible due to the fact that enantioselectivity and turnover number are dominated by different microscopic rate constants.

REFERENCES

1. Lutje Spelberg, J. H., van Hylckama Vlieg, J. E. T., Tang, L., Janssen, D. B., and Kellogg, R. M. (2001) Highly enantioselective and regioselective biocatalytic azidolysis of aromatic epoxides, *Org. Lett. 3*, 41−43.
2. Lutje Spelberg, J. H., Tang, L., van Gelder, M., Kellogg, R. M., and Janssen, D. B. (2002) Exploration of the biocatalytic potential of a halohydrin dehalogenase using chromogenic substrates, *Tetrahedron: Asymmetry 13*, 1083−1089.
3. van den Wijngaard, A. J., Janssen, D. B., and Witholt, B. (1989) Degradation of epichlorohydrin and halohydrins by bacterial cultures isolated from freshwater sediment, *J. Gen. Microbiol. 135*, 2199−2208.
4. Nakamura, T., Nagasawa, T., Yu, F., Watanabe, I., and Yamada, H. (1991) A new catalytic function of halohydrin hydrogen-halide-lyase, synthesis of β-hydroxynitriles from epoxides and cyanide, *Biochem. Biophys. Res. Commun. 180*, 124−130.
5. Poelarends, G. J., van Hylckama Vlieg, J. E. T., Marchesi, J. R., Freitas dos Santos, L. M., and Janssen, D. B. (1999) Degradation of 1,2-dibromoethane by *Mycobacterium* sp. strain GP1, *J. Bacteriol. 181*, 2050−2058.
6. Marek, J., Vevodova, J., Smatanova, I. K., Nagata, Y., Svensson, L. A., Newman, J., Takagi, M., and Damborsky, J. (2000) Crystal structure of the haloalkane dehalogenase from *Sphingomonas paucimobilis* UT26, *Biochemistry 39*, 14082−14086.
7. Newman, J., Peat, T. S., Richard, R., Kan, L., Swanson, P. E., Affholter, J. A., Holmes, I. H., Schindler, J. F., Unkefer, C. J., and Terwilliger, T. C. (1999) Haloalkane dehalogenases: Structure of a *Rhodococcus* enzyme, *Biochemistry 38*, 16105−16114.
8. Ridder, I. S., Rozeboom, H. J., Kalk, K. H., and Dijkstra, B. W. (1999) Crystal structures of intermediates in the dehalogenation of haloalkanoates by L-2-haloacid dehalogenase, *J. Biol. Chem. 274*, 30672−30678.
9. Verschueren, K. H., Seljee, F., Rozeboom, H. J., Kalk, K. H., and Dijkstra, B. W. (1993) Crystallographic analysis of the catalytic mechanism of haloalkane dehalogenase, *Nature 363*, 693−698.
10. Benning, M. M., Taylor, K. L., Liu, R.-Q., Yang, G., Xiang, H., Wesenberg, G., Dunaway-Mariano, D., and Holden, H. M. (1996) Structure of 4-chlorobenzoyl coenzyme A dehalogenase determined to 1.8 Å resolution: an enzyme catalyst generated via adaptive mutation, *Biochemistry 35*, 8103−8109.
11. de Jong, R. M., and Dijkstra, B. W. (2004) Structure and mechanism of bacterial dehalogenases: different ways to cleave a carbon−halogen bond, *Curr. Opin. Struct. Biol. 13*, 722−730.
12. Lutje Spelberg, J. H., van Hylckama Vlieg, J. E. T., Bosma, T., Kellogg, R. M., and Janssen, D. B. (1999) A tandem enzyme reaction to produce optically active halohydrins, epoxides and diols, *Tetrahedron: Asymmetry 10*, 2863−2870.
13. Van Hylckama Vlieg, J. E. T., Tang, L., Lutje Spelberg, J. H., Smilda, T., Poelarends, G. J., Bosma, T., van Merode, A. E. J., and Janssen, D. B. (2001) Halohydrin dehalogenases are structurally and mechanistically closely related to short-chain dehydrogenases/reductases, *J. Bacteriol. 183*, 5058−5066.
14. de Jong, R. M., Tiesinga, J. J. W., Rozeboom, H. J., Kalk, K. H., Tang, L., Janssen, D. B., and Dijkstra, B. W. (2003) Structure and mechanism of a bacterial haloalcohol dehalogenase: a new variation of the short-chain dehydrogenase/reductase fold without an NAD(P)H binding site, *EMBO J. 22*, 4933−4944.
15. Jörnvall, H., Persson, B., Krook, M., Atrian, S., Gonzalez-Duarte, R., Jeffery, J., and Ghosh, D. (1995) Short-chain dehydrogenases/reductases (SDR), *Biochemistry 34*, 6003−6013.
16. Hwang, C. C., Chang, Y. H., Hsu, C. N., Hsu, H. H., Li, C. W., and Pon, H. I. (2004) Mechanistic roles of Ser114, Tyr155 and Lys159 in 3α-hydroxysteroid dehydrogenase/carbonyl reductase from *Comamonas testossteroni*, *J. Biol. Chem*. (in press).
17. Tang, L., Lutje Spelberg, J. H., Fraaije, M. W., and Janssen, D. B. (2003) Kinetic mechanism and enantioselectivity of halohydrin dehalogenase from *Agrobacterium radiobacter*, *Biochemistry 42*, 5378−5386.
18. Tang, L., van Merode, A. E. J., Lutje Spelberg, J. H., Fraaije, M. W., and Janssen, D. B. (2003) Steady-state kinetics and tryptophan fluorescence properties of halohydrin dehalogenase from *Agrobacterium radiobacter*. Roles of W139 and W249 in the active site and halide-induced conformational change, *Biochemistry 42*, 14057−14065.
19. Westkaemper, R. B., and Hanzlik, R. P. (1981) Mechanistic studies of epoxide hydrolase utilizing a continuous spectrophotometric assay, *Arch. Biochem. Biophys. 208*, 195−204.
20. Rink, R., Fennema, M., Smids, M., Dehmel, U., and Janssen, D. B. (1997) Primary structure and catalytic mechanism of epoxide hydrolase from *Agrobacterium radiobacter* AD1, *J. Biol. Chem. 272*, 14650−14657.
21. Tang, L., Van Hylckama Vlieg, J. E. T., Lutje Spelberg, J. H., Fraaije, M. W., and Janssen, D. B. (2002) Improved stability of halohydrin dehalogenase from *Agrobacterium radiobacter* AD1 by replacement of cysteine residues, *Enzyme Microb. Technol. 30*, 251−258.
22. Bergmann, J. G., and Sanik, J. (1957) Determination of trace amounts of chlorine in naphtha, *Anal. Chem. 29*, 241−243.
23. Johnson, K. A. (1992) *The Enzymes* (Boyer, P. D., Ed.) 4th ed., Vol. 20, pp 1−60, Academic Press, New York.
24. Huang, C. Y. (1979) Derivation of initial velocity and isotope exchange rate equations, *Methods Enzymol. 63*, 54−84.
25. Johnson, K. A. (1986) Rapid kinetic analysis of mechanochemical adenosine-triphosphatases, *Methods Enzymol. 134*, 677−705.
26. Schanstra, J. P., and Janssen, D. B. (1996) Kinetics of halide release of haloalkane dehalogenase: evidence for a slow conformational change, *Biochemistry 35*, 5624−5632.
27. Pries, F., Van den Wijngaard, A. J., Bos, R., Pentenga, M., and Janssen, D. B. (1994) The role of spontaneous cap domain mutations in haloalkane dehalogenase specificity and evolution, *J. Biol. Chem. 269*, 17490−17494.
28. Rüdiger, M., and Oesterhelt, D. (1997) Specific arginine and threonine residues control anion binding and transport in the light-driven chloride pump halorhodopsin, *EMBO J. 16*, 3813−3821.
29. Schanstra, J. P., Ridder, A., Kingma, J., and Janssen, D. B. (1997) Influence of mutations of Val226 on the catalytic rate of haloalkane dehalogenase, *Protein Eng. 10*, 53−61.

30. Rotticci, D., Rotticci-Mulder, J. C., Denman, S., Norin, T., and Hult, K. (2001) Improved enantioselectivity of a lipase by rational protein engineering, *ChemBioChem 2*, 766−770.
31. Chen-Goodspeed, M., Sogorb, M. A., Wu, F., and Raushel, F. M. (2001) Enhancement, relaxation, and reversal of the stereoselectivity for phosphotriesterase by rational evolution of active site residues, *Biochemistry 40*, 1332−1339.

BI047613Z